

# Super-resolution Rydberg imaging reaching the nanoscale

Xiaoguang Huo<sup>1</sup>, J. F. Chen<sup>2,3,†</sup>, Jing Qian<sup>1,\*</sup>

<sup>1</sup>*State Key Laboratory of Precision Spectroscopy,  
Department of Physics, School of Physics and Material Science,  
East China Normal University, Shanghai 200062, China*

<sup>2</sup>*Guangdong Provincial Key Laboratory of Quantum Science and Engineering,  
Southern University of Science and Technology, Shenzhen, 518055, China and*

<sup>3</sup>*Shenzhen Institute for Quantum Science and Engineering,  
Southern University of Science and Technology, Shenzhen, 518055, China\**

(Dated: October 26, 2020)

We present a scheme for the nondestructive and ultra-sensitive imaging of Rydberg atoms within an ensemble of cold probe atoms. This is made possible by the interaction-enhanced electromagnetically induced transparency at off-resonance which enables an extremely narrow zero-absorption window for an enhanced 100% transmission. By probing the transmission rate we obtain the distribution of Rydberg atoms with both ultra-high spatial resolution and fast response, ensuring a precise real-time imaging. Increased resolution compared to previous work allows us to accurately obtain the information of atom position at the nanometer scale via adjusting the probe detuning only. This new type of interaction enhanced transmission imaging can be utilized to other impure systems containing strong many-body interactions, and is promising to develop nanoscale super-resolution microscopy.

## I. INTRODUCTION

The demand for imaging individual Rydberg atoms with high spatial and temporal resolutions gave birth to the development of versatile optical imaging techniques. Earlier methods accessible for that purpose were based on, *e.g.*, the field ionization imaging [1, 2] or fluorescence imaging [3, 4] of atoms uncovering both virtues. However these detection methods are destructive and the atoms cannot be re-used. For showing important applications in diverse areas, such as the quantum information processing [5], a nondestructive and high-efficiency detection of Rydberg states is imperative. Recently, a superconducting microwave cavity has been used for efficient single-shot nondestructive measurement of Rydberg-atom ensembles enabled by its enhanced sensitivity, opening up new perspectives for imaging Rydberg atoms [6].

Alternatively a promising approach proposed by refs. [7, 8], is the interaction enhanced imaging (IEI) which manifests as a nondestructive and state-selective optical detection of strongly interacting impurities. Over the last decade IEI has been actively pursued by experimental devotion in versatile systems [9, 10] as a new protocol for investigating the readout of the time-resolved dynamics of ions [11] or molecules [12], the generation of single-photon transistor with high gain [13] and various long-range interactions [14, 15]. IEI underlyingly relies on the strong impurity-probe interaction in the vicinity of each impurity, which can induce an enhanced absorption imaging in the case of resonant electromagnetically

induced transparency (EIT) [16–18]. By mapping this strong interaction onto the light field one can resolve the property of each impurity without destroying it. However as for Rydberg impurities, their spatial response range is limited by the Rydberg blockade radius, typically around a few micrometers [19–21]. Reducing it down to the level of nanometer scale has to be at expense of a strong coupling laser, which is still challenging for current experimental implementation.

In this work we develop a new protocol of IEI by considering it in an off-resonant EIT environment, which benefits from a very narrow 100%-transmission window, consequently named as interaction enhanced *transmission* imaging (IETI). This window is caused by the compensation between a big probe-atom detuning at off resonance and the strong impurity(target)-probe interaction, whose width can be flexibly adjusted to be orders of magnitude narrower than a typical blockade radius. By carrying out such an off-resonant measurement with respect to the probe atoms, it is feasible to obtain a spatially resolved imaging of random Rydberg targets, accompanied by a fast optical response in real-time detection. Increased resolution below 100nm in IETI, can facilitate accurate and quick positioning of atoms, especially when multi-Rydberg atoms overlap within a specific region. The scheme is deserving a future experimental exploration for the realization of nanoscale super-resolution microscopy.

## II. THEORETICAL STRATEGY

---

\* jqian1982@gmail.com

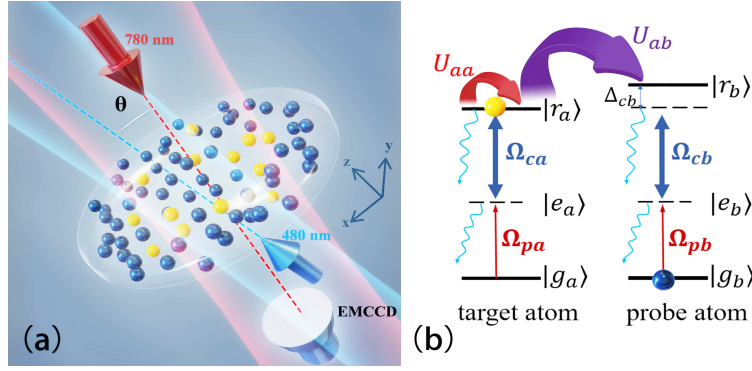


FIG. 1. (a) Sketch for the super-resolution imaging of Rydberg targets by the way of IETI. Target atoms (yellow) are randomly embedded within an ensemble of dense quasi-two-dimensional probe atoms (blue) in  $x-y$  plane. Both atoms interact with two light fields (probe and coupling) propagating in  $-z$  and  $+z$  directions respectively, which enable a two-photon transition from the ground state  $|g_{a(b)}\rangle$  to the Rydberg state  $|r_{a(b)}\rangle$  via middle states  $|e_{a(b)}\rangle$ . The probe and coupling lasers with wavelengths 780nm and 480nm, can induce a negligible Doppler shift as they are almost vertical to the stochastic atomic movements in  $x-y$  plane. By detecting the probe-field transmission at the end of  $-z$  axis with an EMCCD camera all target atom positions could be precisely resolved. In detection, in order to reduce the impact of coupling laser there exists a tiny intersection angle  $\theta \leq 5^\circ$  between the probe and coupling fields. (b) Relevant energy levels and atom-field interactions of the target and probe atoms. The strong probe-target interactions  $U_{ab}$  will overcome the big detuning  $\Delta_{cb}$  with respect to state  $|r_b\rangle$ , arising a sharp 100%-transmission window at a special probe-target spacing.  $U_{aa}$  reflects the strength of target-target interaction.

The principle of our approach is illustrated in Fig.1 where a few target atoms randomly embedding in a quasi-two-dimensional system, are surrounded by a large number of background probe atoms. Initially given ground target atoms, the probe atom coupled by light fields  $\Omega_{pb}$  and  $\Omega_{cb}$  will suffer from an inefficient excitation due to the presence of a big off-resonant detuning  $\Delta_{cb} \gg \Omega_{pb}, \Omega_{cb}$ . However, once the target atoms are prepared on Rydberg state  $|r_a\rangle$  through a cycling two-photon pumping with Rabi frequencies  $\Omega_{pa}$  and  $\Omega_{ca}$ , the induced probe-target interaction  $U_{ab}$  acts as an effective detuning for  $|r_b\rangle$ . Here  $U_{ab} = -C_3/R^3$  [22, 23] forms as an attractive dipole-dipole-type where  $C_3$  is the dispersion coefficient and  $R$  reflects the distance to the target-probe interaction. The presence of  $U_{ab}$  possibly overcomes  $\Delta_{cb}$  with respect to the probe atom, and thus gives rise to a spatial EIT effect. Therefore the position of such random target atoms can be spatially resolved via a very narrow EIT transmission window at off-resonance [24]. To describe the probe-atom absorption that undergoes an off-resonant EIT excitation, the Hamiltonian describing single probe atom is given by

$$\mathcal{H}_b = \frac{1}{2}(\Omega_{pb}|e\rangle\langle g|_b + \Omega_{cb}|r\rangle\langle e|_b + H.c.) + \Delta'_{cb}|r\rangle\langle r|_b. \quad (1)$$

Noting that the presence of an excited target atom will cause a finite energy shift  $U_{ab}$  to state  $|r_b\rangle$ , which has been effectively translated into a two-photon detuning  $\Delta'_{cb} = \Delta_{cb} + U_{ab}$ . For probe atoms due to the tiny excitation probability at far off-resonance one has ignored the many-body interactions  $U_{bb}$ . Besides the target-target interaction  $U_{aa}$  plays role only if more than two target atoms are coupled to state  $|r_a\rangle$  at the same time, and will leave for consideration in the many-atom imaging.

Here we begin with a detailed analysis for the case of single target atom. By taking account into the spontaneous decays  $\Gamma_{eb}, \Gamma_{rb}$  from states  $|e_b\rangle$  and  $|r_b\rangle$ , and following the approach of master equation for the density matrix  $\rho_b$  ( $\rho_{b,ij}$  stands for the matrix element and the subscript  $b$  means the probe atom), we can solve the stationary element  $\rho_{b,eg}$  for describing the probe transition [25],

$$\rho_{b,eg}(r, v)dv = \frac{2\Omega_{pb}(\delta(r) + i\gamma_{rb})}{\Omega_{cb}^2 + 4\gamma_{eb}(\gamma_{rb} - i\delta(r))} \mathcal{N}(v)dv, \quad (2)$$

under the assumption of  $\Omega_{pb} \ll \Omega_{cb}$ ,  $\rho_{gg} \approx 1$ , and  $\gamma_{eb(rb)} = \frac{1}{2}\Gamma_{eb(rb)}$  meaning the relaxation rate. Remarkably in Eq.(2) the new denotation  $\delta(r)$  expressing as

$$\delta(r) = \Delta_{cb} - \frac{C_3}{R^3} - (\vec{k}_c + \vec{k}_p) \cdot \vec{v}, \quad (3)$$

with the probe-target spacing  $R = |r - r_a|$ , represents the effective two-photon detuning and  $r_a$  is the random location of single target atom. Accounting for the thermal motion of probe atoms that translates into a Doppler frequency shift to the atomic internal levels we phenomenologically introduce this effect where  $\mathcal{N}(v)$  in Eq.(2) is the number density of  $^{87}\text{Rb}$  probe atoms with velocity  $v$  and  $k_{c,p} = 2\pi/\lambda_{c,p}$  is the coupling wavevector.  $\mathcal{N}(v)$  takes form of a Maxwell-Boltzmann function at thermal equilibrium. To reduce the impact of Doppler shift we have made two beams propagate nearly vertical to the atom movement, see Fig.1a. To this end, the susceptibility corresponding to the atomic transition driven by the probe field is given by

$$\chi(r, v)dv = \frac{2\mu_{ge}}{\epsilon_0 E_p} n(r) \rho_{b,eg}(r, v)dv, \quad (4)$$

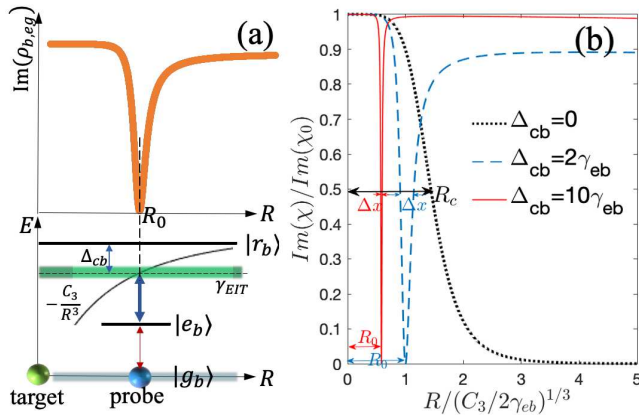


FIG. 2. Imaginary part of  $\rho_{b,eg}(r)$  representing the probe absorption effect. (a) At a special placement with  $\delta(r) = 0$ , it arises a critical distance  $R_0 \approx \sqrt[3]{C_3/\Delta_{cb}}$  at which a narrow zero-absorption window emerges. (b) The absolute absorption  $\text{Im}[\chi]$  normalized by  $\text{Im}(\chi_0) = n_0 \mu_{eg}^2 / (\epsilon_0 \hbar \gamma_{eb})$  vs the relative spacing  $R$  (in unit of  $\sqrt[3]{C_3/2\gamma_{eb}}$ ) under various  $\Delta_{cb}$  values. For  $\Delta_{cb} = 0$  there exists a wider absorption-enhanced window within the Rydberg-blockade volume  $R_c = \sqrt[3]{4\gamma_{eb}C_3/\Omega_{cb}^2}$ , as similar as Fig.2(b) of ref.[8]. However if  $\Delta_{cb} \neq 0$  a narrower zero-absorption dip emerges, which ensures a perfect transmission signal there.

where the Gaussian atomic number density is  $n(r) = n_0 \exp(-r^2/2\sigma_r^2)$  with  $n_0$  the peak and  $\sigma_r$  the half-width.  $E_p$  is the probe electric field amplitude, and  $\epsilon_0$  is vacuum dielectric constant. The real (imaginary) part of the susceptibility  $\chi(r)$  corresponds to the dispersion (absorption) of the probe light, caused by the atomic medium. By integrating the imaginary part of Eq.(4) over the velocity distribution for temperature  $T$  we can obtain an absolute absorption coefficient  $\text{Im}(\chi(r))$  as a function of  $R$ .

Figure 2 illustrates the probe absorption effect by calculating the imaginary parts. First we understand the essence of transmission-enhanced imaging by following the map of (a). In the vicinity of an off-resonant driving probe atom, detuned by  $\Delta_{cb}$  with respect to a Rydberg state  $|r_b\rangle$ , the energy level of  $|r_b\rangle$  is also shifted by the strong probe-target potential  $U_{ab} = -C_3/R^3$ . Here  $r_a = 0$  and  $R = |r|$  are assumed. If satisfying  $\Delta_{cb} - C_3/R^3 \approx 0$  and  $\Delta_{cb} \neq 0$  one can obtain a zero-absorption window at  $R_0 \approx \sqrt[3]{C_3/\Delta_{cb}}$  with its width  $\Delta x$  much smaller than the blockade radius  $R_c$ . The strength of Doppler shift  $(\vec{k}_c + \vec{k}_p) \cdot \vec{v}$  can be made orders of magnitude smaller than the Rydberg shift  $U_{ab}$ . For example a rough estimation based on the wavevector  $k_c = 13.1 \mu\text{m}^{-1}$  ( $\lambda_c = 480\text{nm}$ ),  $k_p = 8.1 \mu\text{m}^{-1}$  ( $\lambda_p = 780\text{nm}$ ) and the most probable speed  $v = \sqrt{\frac{2kT}{m}} = 6.2\text{cm/s}$ , gives rise to a maximal value for describing the Doppler shift, which is  $(k_c + k_p)v \approx 1.3\text{MHz} \ll |U_{ab}|$ . In fact  $\vec{k}_{c,p}$  is almost vertical to  $\vec{v}$  in our scheme, leading to a per-

fect Doppler-free measurement. So  $\delta(r) \approx \Delta_{cb} - C_3/R^3$  is confirmed. The resulting enhanced probe transmission can precisely reflect the position of the target atom. This high-contrast and high-precise transmission signal could be suited for the target atom imaging.

However if  $\Delta_{cb} = 0$  as in traditional IEI schemes[7, 8], the absorption response manifests as an opposite change. As  $R \rightarrow \infty$  the excited state  $|r_b\rangle$  becomes far-detuned and suffers from a zero absorption. Yet within the blockade radius  $R_c$ , *i.e.*,  $R < R_c = \sqrt[3]{4\gamma_{eb}C_3/\Omega_{cb}^2}$ , an enhanced absorption can return a well signature for imaging the location of the target Rydberg atom, although the spatial resolution is relatively poor. Because the broad absorption linewidth determined by  $R_c$  makes the position measurement insensitive. As a consequence it is insufficient for achieving an ultraprecise microscopic imaging of individual atoms by using traditional IEI technology.

A quantitative verification for different probe absorption rates is comparably illustrated in Fig.2b. It is clearly shown that the resonant case of  $\Delta_{cb} = 0$  (black-dotted) allows for an absorption-enhanced signal with its half-width  $R_c$  at half-maximum. However our approach using  $\Delta_{cb} \neq 0$  (blue-dashed and red solid) greatly benefits from an ultraprecise spatial resolution, characterized by the extremely narrow width  $\Delta x$ , which is given by

$$\Delta x \approx \left(\frac{C_3}{\Delta_{cb} - \frac{\Omega_{cb}^2}{4\gamma_{eb}}}\right)^{1/3} - \left(\frac{C_3}{\Delta_{cb} + \frac{\Omega_{cb}^2}{4\gamma_{eb}}}\right)^{1/3} \quad (5)$$

occurring at the zero-absorption dip  $R = R_0$ . At that place a 100% transmission probability can be obtained.  $\Delta x$  is easily tunable by the detuning  $\Delta_{cb}$ , and in principle  $\Delta_{cb} \gg \frac{\Omega_{cb}^2}{4\gamma_{eb}}$  will lead to arbitrary scale of spatial resolution because  $\Delta x \rightarrow 0$  as long as the contrast of images permits. Such a narrower zero-absorption window could deeply improve the imaging precision for the target atoms, promising the development of a super-resolution atom microscopy.

### III. SINGLE-TARGET-ATOM IMAGING

#### A. High spatial resolution

To carry out numerical calculations for the EIT imaging of random-embedded target atoms, all the probe-target and target-target interactions have to be considered. This is a many-body problem. In our calculation, we simulate a cyclic excitation with respect to the target atoms which have been prepared on the ground state initially. The Rydberg excitation of target atoms will return a significant change to the EIT absorption of surrounding probe atoms. By detecting this probe-atom EIT signal the target-atom position can be precisely resolved.

In a practical experiment, given by the ground atoms one has to prepare all target atoms onto their Rydberg states through a cyclic excitation process. Numerical preparation for target atoms has been described in appendix A. Here we simply consider the case of single tar-

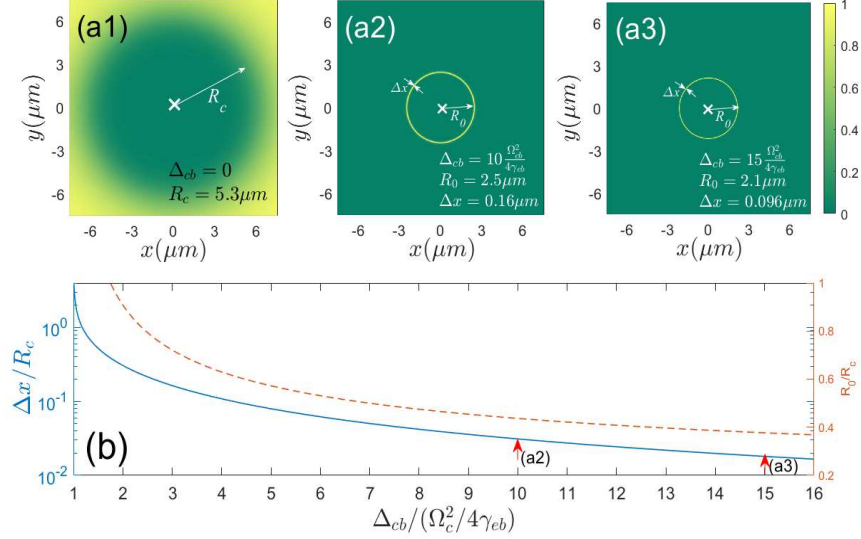


FIG. 3. (a1-a3) Transmission imaging of the single target atom surrounded by dense probe atoms. The unique target atom locates at the center  $x = y = 0$ , denoted by a white cross. In (a1),  $\Delta_{cb} = 0$  as used in earlier works the spatial resolution  $R_c$  is decided by the half-width of transmission which is smoothly increasing as  $r = \sqrt{x^2 + y^2}$  grows; in (a2-a3) choosing  $\Delta_{cb} > \Omega_{cb}^2/4\gamma_{eb}$  arises a very narrow ring-shaped transmission window at  $r = R_0$  which serves a more precise determination for the position of target atom, arising from its higher spatial resolution decided by its width  $\Delta x \ll R_c$ . (b) The ratio  $\Delta x/R_c$  (blue-solid) vs  $\Delta_{cb}$  represents a significant decreasing tendency. For a larger  $\Delta_{cb}$  it is possible to reach a nanoscale microscopic imaging below 100nm *e.g.*  $\Delta x = 95.6\text{nm}$  in (a3). The red-dashed line shows the ratio  $R_0/R_c$  continuously decreases and is always smaller than 1.0 as  $\Delta_{cb}$  increases. Red arrows point to the parameters used in (a2) and (a3).

get atom at a determined position  $r_a$  which has been prepared on Rydberg state  $|r_a\rangle$  before imaging. The presence of such an excited target atom can modify  $\delta(r)$  of the probe atoms, as defined in Eq.(3), returning an enhanced transmission signal for the probe light. It happens when  $|r - r_a| = R_0$  is met. In numerical simulation we assume it has been pre-excited by denoting  $\{\rho_{a,rr}\} \equiv 1$ . Other parameters are as follows. A quasi-2D atomic ensemble with ultracold  $^{87}\text{Rb}$  atoms at  $10\mu\text{K}$ , serves as the probe atoms. The peak atomic density is  $n_0 = 8 \times 10^8 \text{mm}^{-3}$  and radially follows a Gaussian density distribution with a half-width  $\sigma_r = 0.7\text{mm}$  [21]. The unique target atom placed in the center is also rubidium atom. The experimental energy levels are  $|g_b\rangle = |5S_{1/2}, F = 2, m_F = 2\rangle$ ,  $|e_b\rangle = |5P_{3/2}, F = 3, m_F = 3\rangle$ , and  $|r_b\rangle = |37S_{1/2}, m_J =$

$1/2\rangle$  for the probe atom; and  $|r_a\rangle = |50S_{1/2}\rangle$  for the target atom [9]. The dipole-dipole coefficient is  $C_3/2\pi = 1.6 \text{GHz}\cdot\mu\text{m}^3$ . The decay rates are chosen to be  $\Gamma_{eb}/2\pi = 5.4\text{MHz}$  and  $\Gamma_{rb}/2\pi = 3.6\text{kHz}$  [26]. For realizing an EIT excitation the Rabi frequencies of probe atoms are  $\Omega_{pb}/2\pi = 0.54\text{MHz}$  and  $\Omega_{cb}/2\pi = 10.8\text{MHz}$ . With the above experimentally-accessible parameters, transforming into the frame of probe transmission one follows [16]

$$T(x, y) = |\exp\{ik_p L_z \chi(x, y)/2\}| \quad (6)$$

in order to show the transmission spectra where  $k_p$  is the probe wavevector and  $L_z = 10\mu\text{m}$  is the z-axis medium thickness. For realizing a quasi-2D system we use  $L_z < L_{x,y}$ . In plotting transmission  $T$  we reduce it into the form of  $T \sim \exp[i\eta n(x, t)\rho_{b,eg}(x, y)]$  with a dimensionless pre-coefficient  $\eta = k_p L_z \mu_{ge} n_0 / \epsilon_0 E_p \approx 39.4$ .

As displayed in Fig.3(a1-a3) our single target atom transmission imaging is represented within an amplified  $(15 \times 15)\mu\text{m}^2$  area. Each pixel corresponds to a region of  $(0.015\mu\text{m})^2$ . For  $\Delta_{cb} = 0$  the location of the unique target atom denoted by white cross, can be resolved in a broad disk area with its radius  $R_c \approx 5.3\mu\text{m}$ , which is equivalent to a typical blockade range. However if a nonzero  $\Delta_{cb}/2\pi = (108, 162)\text{MHz}$  is applied, as shown in (a2-a3), one can easily envisage higher resolution given

by an enhanced transmission quality with a spatial extent even below 100nm, by which a nondestructive detection for the central target atom is achievable. It is clearly shown that both contrast and spatial resolution of our IETI approach are greatly improved as compared to the way of IEI with  $\Delta_{cb} = 0$ . Surely a higher spatial resolution is principally satiable by a growing  $\Delta_{cb}$  yet at expense of image contrast. So in order to obtain a visible image we will adopt the best parameters in (a3)

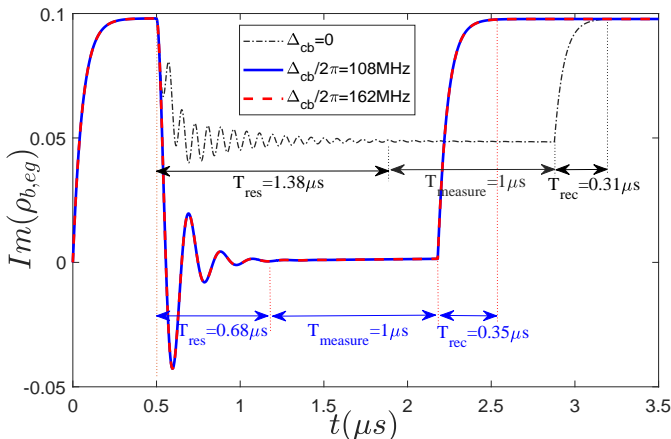


FIG. 4. Transient behavior of probe absorption  $Im(\rho_{b,eg}(t))$  as a function of  $t$  in the Rydberg EIT via a sudden switch-on of the coupling laser at  $t = 0.5\mu s$  and a sudden-off of it after undergoing a  $1.0\mu s$  steady measurement. By using different  $\Delta_{cb}$  values, the total single imaging time contains response time  $T_{res}$ , stable measurement  $T_{measure}$ , recover time  $T_{rec}$ , are separately denoted.

for studying the many-atom case. Figure 3(b) confirms that the ratio  $\Delta x/R_c$  illustrating the improved strength of the spatial resolution, can be made even smaller via an adjustment of  $\Delta_{cb}$ . And at the same time the annulus radius  $R_0$  in IETI can also be shrunk into almost half of the blockade radius  $R_c$  as long as  $\Delta_{cb}$  is appropriately chosen, giving a promising way for an ultra-precise determination of atom location from the IETI technique.

### B. Fast response in real-time imaging

A continuous imaging beam could cause a stationary measurement for Rydberg targets; however once the control or probe field switches with time, it requires a finite response time that the system reaches a new equilibrium. This response speed of Rydberg EIT could qualify the property of the real-time imaging. So far a fast response property of Rydberg EIT has been verified to be facilitated by the presence of strong Rydberg-Rydberg interactions [27, 28]. We numerically study the real-time absorption behavior of the probe atoms at a determined distance  $R_0$  which could reflect the least time required for single measurement. The initial probe atoms are assumed to undergo a sudden switch-on of the coupling field  $\Omega_{cb}(t)$ , consequently attaining a stationary state during the imaging process. But once the coupling laser is switched off after single stable measurement, the system tends to recover accompanied by a different recovering time. We can roughly estimate the least time for single measurement which should contain three processes of response, recover and stable measurement. A faster response time could improve the imaging quality, accelerating single real-time detection in experiment. Figure 4

comparably shows the transient behavior at on-resonance or at far-off resonance. In the calculation, by switching on the coupling laser  $\Omega_{cb}(t)$  at  $t = 0.5\mu s$ , the probe absorption  $Im(\rho_{b,eg}(t))$  tends to be stationary onto new status with different speeds. It is clear that before the switch-on of  $\Omega_{cb}(t)$ ,  $Im(\rho_{b,eg}(t))$  is same for all cases due to the decoupled state  $|r_b\rangle$ . However once  $\Omega_{cb}(t)$  is present the frequency shift of  $|r_b\rangle$  will strongly impact the probe absorption. For  $\Delta_{cb} = 0$  this shift solely caused by the strong probe-target interaction  $U_{ab}$ , will lead to a long response time with strong oscillations towards the steady state, typically much larger than  $1\mu s$ . Fortunately when  $U_{ab}$  is exactly overcome by a finite  $\Delta_{cb}$  as applied in our scheme, an effective resonant excitation with  $\Delta'_{cb} = 0$  for the probe atoms could favor a fast response time  $\sim 0.68\mu s$  to be stationary. A numerical criterion for stationary state in the calculation is estimated by an average fluctuation of absorption within a time period of  $0.1\mu s$  that meets the condition of  $|\delta Im(\rho_{b,eg})| < 10^{-3}$ . This perfect compensation is regardless of the exact  $\Delta_{cb}$  values, so different  $\Delta_{cb}$  give rise to exactly same transient behaviors. Due to the fast response time by an off-resonance spatial EIT we can safely assume that the atoms are nearly stationary during the imaging process.

After the fast EIT response we set a same time period  $1\mu s$  for carrying out the stable measurement. Then the coupling field  $\Omega_{cb}(t)$  is turned off again, arising a similar recovering time back to the original status. Therefore the single measurement requires at least  $T_{res} + T_{meas} + T_{rec} \approx 2\mu s$  in our scheme which could be also regarded as the temporary resolution. To our knowledge in a real-time imaging process such measurement with fast response can be performed by monitoring the stationary images using a suitable detector, *e.g.* EMCCD [11]. Such detector has shown its preeminent ability in the weak-field measurement because of its ultra-low noise, high resolution, high-quantum efficiency, and the robustness to overexposure [29, 30].

## IV. MANY-ATOM IMAGING

For the case with more target atoms, we have to perform a many-body quantum simulation following the stationary probability  $\rho_{b,eg}(r)$  of each probe atom. Detailed simulation procedures are described in the appendix A. In Fig.5 we present the transmission images of probe atoms for resolving the critical position of target atom  $i$ . Note that all probe-target  $U_{ab}$  and target-target  $U_{aa}$  interactions play roles in the calculation. The former produced by the energy shift of probe Rydberg states can be overcome via an off-resonance detuning  $\Delta_{cb}$ , giving a precise positioning of the target atoms, while the latter decides the Rydberg-state probability of target atoms. Repeated optical repumping technique with Rabi frequencies  $\Omega_{pa} \gg \Omega_{ca}$  ensures a higher excitation probability on average. Once they are kept sustaining on state  $|r_a\rangle$  it leads to  $\{\rho_{a,rr}^i\} = 1$ , in analogy to the single target

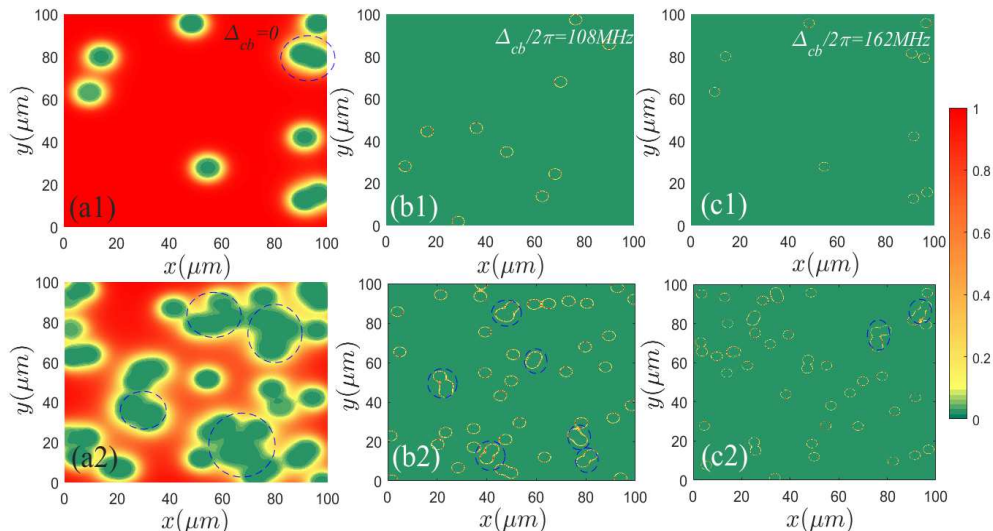


FIG. 5. (color online) Simulated many-atom transmission imaging with 10 [a1-c1] and 50 [a2-c2] randomly-distributed target atoms, respectively. By increasing the detuning  $\Delta_{cb}/2\pi = (0, 108, 162)$  MHz, the transmission images for many atoms become more distinguishable with higher spatial resolution, accounting for the dual realization of  $R_0 < R_c$  and  $\Delta x \ll R_c$  in IETI. The excitation laser for the target atom is arbitrary, but a nearly perfect Rydberg probability of target atoms occurs as long as the exciting time is sufficient. Here  $(\Omega_{ca}, \Omega_{pa})/2\pi = (5.4, 54)$  MHz for the Rabi frequencies of target excitation and the pre-coefficient  $C_6/2\pi = 3.8 \text{ MHz} \cdot \mu\text{m}^6$  used for calculating the van der Waals-type interaction between two target atoms which is  $U_{aa} = C_6/r_{aa}^6$ .

atom case where the atom's position could be precisely resolved. During the  $n$ th measurement the time for stationary transmission has been considered. Due to the low temperature as well as fast response we safely assume all target and probe atoms have been stationary during the imaging process. A discussion for the real-time evolution of probe absorption within single measurement is presented in Sec.III.B.

Figure 5 globally illustrates the transmission images of random 10 or 50 atoms distributed over a wide area of  $(100 \times 100) \mu\text{m}^2$ . With the traditional IEI method each target atom can be resolved by detecting the zero-transmission (full-absorption) window of probe EIT, yet suffering from a big reduction of spatial resolution if  $N_A$  (the number of target atoms) is large. Because the image spots decided by the blockade radius  $R_b$  significantly overlap in space as  $N_A$  becomes larger and this leads to a poor resolution, as shown within dashed cir-

cles in (a2). Luckily, by tuning  $\Delta_{cb}$  to be a nonzero value as proposed by us in the new way of IETI, here  $\Delta_{cb}/2\pi = (108, 162) \text{ MHz}$  is used, the quality for atomic imaging obtains a great improvement. That fact is mainly caused by a full-probe transmission in IETI accompanied by a flexible target-probe spacing  $R_0$  that depends on  $\Delta_{cb}$ . In Fig.5(b-c) it is clearly shown that the virtue of IETI lies in that both  $R_0$  and its fluctuated extent  $\Delta x$  can be freely tunable by the detuning  $\Delta_{cb}$  only, allowing for  $R_0 < R_c$  and  $\Delta x \ll R_c$ . Consequently as comparing (a2) with (b2-c2) we see it is quite difficult to distinguish nearby atoms when  $\Delta_{cb} = 0$ ; however in IETI the presence of a narrow and sharp transmission window powerfully enables a super-resolution measurement of atomic positions which can persist a high-quality transmission imaging of even 50 atoms within same detection area.

## V. CONCLUSION

We propose an improved IETI technique for the non-destructive determination of atom positions with ultra-high spatial resolution and fast response time. This increased resolution compared to previous IEI method mainly attributes to the use of an off-resonant spatial EIT excitation with respect to the background probe atoms. Once the probe detuning of Rydberg levels suitably overcomes the strong probe-target interaction, it induces a

100% probe transmission window at a critical probe-target distance. One can precisely resolve the location of the target atoms by using this narrow window, attaining a spatial fluctuation below 100 nm. Furthermore, a higher resolution is expected in the IETI approach via the adjustment of detuning solely.

The IETI approach, not only preserves the merits of traditional IEI methods that is a non-destructive and state-sensitive technique, but also provides the possibility for super-resolution Rydberg imaging ascribed to the new

control knob from an off-resonance EIT excitation to the background probe atoms. The response time for single measurement also obtains a great improvement in IETI which is suitable for a present practical performance. All the parameters we use to optimize the simulated images closely meet with the current experimental conditions, deserving for an experimental exploration with cold Rydberg atoms in a practical ensemble.

## ACKNOWLEDGMENTS

J. Qian is supported by the NSFC under Grants No. 11474094 and No. 11104076, by the Science and Technology Commission of Shanghai Municipality under Grant No. 18ZR1412800. J. F. Chen is supported by Grant No.2019ZT08X324 and by Guangdong Provincial Key Laboratory under Grant No.2019B121203002.

### Appendix A: Quantum simulation for many atoms

*Rydberg preparation of target atoms.* The transmission imaging signal can be numerically simulated via a semi-classic Monte Carlo approach [31, 32]. Given the initial status with all target atoms in the ground states  $|g_a\rangle$  we assume an initial one-dimensional array for denoting their status

$$\{\{\rho_{a,rr}^i\}\}_{n=0} = \{0, 0, 0, \dots, 0, 0, \dots\} \quad (\text{A1})$$

where the superscript  $i$  represents the  $i$ th embedded target atom, and  $\{\rho_{a,rr}^i\} = 1$  or  $0$  means that the target atom is excited to  $|r_a\rangle$  or not. The stationary Rydberg probability  $\rho_{a,rr}^i$  of the  $i$ th atom at initial step  $n = 0$  is expressed as [33]

$$\rho_{a,rr}^i \approx \frac{|\Omega_{pa}|^2 (|\Omega_{pa}|^2 + |\Omega_{ca}|^2)}{(|\Omega_{pa}|^2 + |\Omega_{ca}|^2)^2 + (\gamma_{ea}^2 + 2|\Omega_{pa}|^2)\delta_0^2}, \quad (\text{A2})$$

where a resonant two-photon detuning  $\delta_0 = \Delta_{pa} + \Delta_{ca} = 0$  is considered. No target-target interaction presents initially.

Next one generates a random number  $s_i$  between  $(0, 1)$  for each target atom  $i$ . If  $s_i \leq \rho_{a,rr}^i$  we set  $\{\rho_{a,rr}^i\} = 1$  (excited), otherwise,  $\{\rho_{a,rr}^i\} = 0$  (not excited). That will give rise to a new array for example  $\{\{\rho_{a,rr}^i\}\}_n = \{0, 1, 0, 0, \dots, 0, 1, 0, 1, 0, \dots\}$  with  $n = 1, 2, \dots, n_{max}$  representing the iterations.  $\{\{\rho_{a,rr}^i\}\}_n$  denotes the updated status of all target atoms. For the  $i$ th excited target atom *i.e.*  $\{\rho_{a,rr}^i\} = 1$  the nearby target atoms  $j$  in the Rydberg state  $|r_a\rangle$  will induce a target-target level shift, translating into the  $i$ th-atom two-photon detuning  $\delta_i$  given by

$$\delta_i^{(n+1)} = \delta_i^n + \sum_{j \neq i}^{N_A} \{\rho_{a,rr}^j\}_n \frac{C_6}{|r_j - r_i|^6}, \quad (\text{A3})$$

For the initial step  $n = 0$ , and  $\delta_i^{(0)} = \delta_0$ .  $N_A$  is the number of target atoms and  $\frac{C_6}{|r_j - r_i|^6}$  stands for the intraspecies *vdWs* interaction between  $i - j$  target atoms. The target-target interaction can affect the speed towards stable full excitation. Finally a large number of target atoms are prepared on  $|r_a\rangle$ , giving to *e.g.*

$$\{\{\rho_{a,rr}^i\}\}_{n_{max}} = \{1, 1, 1, \dots, 0, 1, \dots\} \quad (\text{A4})$$

under sufficient iterations. The maximum  $n_{max}$  depends on the excitation parameters used for target atoms. In particular, when two or more target atoms are initially closely placed within the blockade radius  $\sim (4\gamma_{ea}C_6/\Omega_{ca}^2)^{1/6} \approx 1\mu\text{m}$  it is difficult to simultaneously excite them owing to the target blockade effect. As a result, by using sufficient iteration times for Rydberg preparation the final average excitation probability is actually given by  $\bar{\rho}_i = \frac{1}{n_{max}} \sum_{n=1}^{n_{max}} \{\rho_{a,rr}^i\}_n \approx 1$ . Note that if any target atom is remaining non-excited it can not be detected in the imaging process due to the absence of probe-target interaction.

*Imaging for probe transmission.* Given the final excitation status of target atoms we recalculate the stationary probe absorption by following Eq.(2) where the effective two-photon detuning  $\delta(r)$  reflecting the probe-target interaction is replaced by

$$\delta(r) = \Delta_{cb} - \sum_{i(r_i \neq r)}^{N_A} \bar{\rho}_i \frac{C_3}{|r - r_i|^3}, \quad (\text{A5})$$

For any atom  $i$  only the surrounding probe atoms with a suitable relative distance  $|r - r_i|$  that leads to  $\delta(r) \approx 0$ , can reveal a sharp zero-absorption window in the EIT spectra. Other unsuited probe atoms can not be detected. Based on the modified Eq.(2) as well as Eq.(4) it arrives at the first-order susceptibility  $\chi(r)$  whose imaginary part stands for the probe absorption rate. The probe transmission is proportional to  $|\exp(i\chi(r))|$  following Eq.(7). By plotting the probe-atom transmission in the  $(x, y)$  space we reach the information of all excited target atoms. Due to the high-quality images of transmission spectra which contains position-sensitive and great resolution advantages, almost all target atoms can be perfectly resolved during single imaging. The stable exposure time required by a typical detector is about a few  $\mu\text{s}$  so here  $T_{measure} = 1\mu\text{s}$  is assumed.

Therefore in our simulation, all target-target interactions coming from the cycling excitation of target atoms performs only in the target-atom preparation process. Once two random target atoms are closely placed within the blockade range for target atoms, this imperfect Rydberg preparation would make measurement failed. To avoid this, in our preparation we have calculated sufficient excitation iterations and finally obtained an average excitation probability for the target atoms. So in general almost all target atoms can be prepared on Rydberg states. In addition all probe-target interactions are considered as long as the target atoms are fully prepared before imaging. The enhanced transmission signal

closing to 100% emerges at the zero-absorption window due to an off-resonant EIT effect. Differing from previous IEI scheme using resonant EIT the off-resonant EIT condition favors a narrower transmission window which promises higher spatial-resolution images. Note that here the probe-probe interaction is ignored accounting for the poor exciting probability of probe atoms in

an off-resonant EIT. In the calculation we adopt sufficient iterations  $n_{max}$  ensuring the Rydberg excitation of target atoms. So the final results involving the target-target  $vdWs$  as well as the probe-target dipole-dipole interactions, can return accurate positions of random-distributed target atoms in a two-dimensional space.

- 
- [1] A. Schwarzkopf, R. E. Sapiro, and G. Raithel, Imaging spatial correlations of rydberg excitations in cold atom clouds, *Phys. Rev. Lett.* **107**, 103001 (2011).
- [2] P. McQuillen, X. Zhang, T. Strickler, F. B. Dunning, and T. C. Killian, Imaging the evolution of an ultracold strontium rydberg gas, *Phys. Rev. A* **87**, 013407 (2013).
- [3] P. Schauss, M. Cheneau, M. Endres, T. Fukuhara, S. Hild, A. Omran, T. Pohl, C. Gross, S. Kuhr, and I. Bloch, Observation of spatially ordered structures in a two-dimensional rydberg gas, *Nature* **491**, 87 (2012).
- [4] H. Labuhn, D. Barredo, S. Ravets, S. De Leseleuc, T. Macri, T. Lahaye, and A. Browaeys, Tunable two-dimensional arrays of single rydberg atoms for realizing quantum ising models, *Nature* **534**, 667 (2016).
- [5] M. Saffman, T. G. Walker, and K. Mølmer, Quantum information with rydberg atoms, *Rev. Mod. Phys.* **82**, 2313 (2010).
- [6] S. Garcia, M. Stammeier, J. Deiglmayr, F. Merkt, and A. Wallraff, Single-shot nondestructive detection of rydberg-atom ensembles by transmission measurement of a microwave cavity, *Phys. Rev. Lett.* **123**, 193201 (2019).
- [7] B. Olmos, W. Li, S. Hofferberth, and I. Lesanovsky, Amplifying single impurities immersed in a gas of ultracold atoms, *Phys. Rev. A* **84**, 041607(R) (2011).
- [8] G. Günter, M. Robert-de Saint-Vincent, H. Schempp, C. S. Hofmann, S. Whitlock, and M. Weidemüller, Interaction enhanced imaging of individual rydberg atoms in dense gases, *Phys. Rev. Lett.* **108**, 013002 (2012).
- [9] G. Günter, H. Schempp, M. Robert-De-Saint-Vincent, V. Gavryusev, S. Helmrich, C. S. Hofmann, S. Whitlock, and M. Weidemueller, Observing the dynamics of dipole-mediated energy transport by interaction-enhanced imaging, *Science* **342**, 954 (2013).
- [10] V. Gavryusev, M. Ferreira-Cao, A. Kekic, G. Zürn, and A. Signoles, Interaction-enhanced imaging of rydberg p states, *European Physical Journal Special Topics* **225**, 2863 (2016).
- [11] C. Gross, T. Vogt, and W. Li, Ion imaging via long-range interaction with rydberg atoms, *Phys. Rev. Lett.* **124**, 053401 (2020).
- [12] M. Huo, Spatial imaging of the movement of bound atoms to reveal the rydberg molecular bond via electromagnetically induced transparency, *EPL (Europhysics Letters)* **118**, 43001 (2017).
- [13] H. Gorniaczyk, C. Tresp, P. Bienias, A. Paris-Mandoki, W. Li, I. Mirgorodskiy, H. P. Büchler, I. Lesanovsky, and S. Hofferberth, Enhancement of rydberg-mediated single-photon nonlinearities by electrically tuned forster resonances, *Nature Communications* **7**, 12480 (2016).
- [14] F. Engel, T. Dieterle, T. Schmid, C. Tomschitz, C. Veit, N. Zuber, R. Löw, T. Pfau, and F. Meinert, Observation of rydberg blockade induced by a single ion, *Phys. Rev. Lett.* **121**, 193401 (2018).
- [15] Z. Zhang, Y. Peng, C. Li, Z. Jia, and Q. Zeng, Proposal for measurement of the van der waals interaction in a cold rydberg ensemble via electromagnetically induced transparency, *Journal of the Optical Society of America B* **36**, 2216 (2019).
- [16] M. Fleischhauer, A. Imamoglu, and J. P. Marangos, Electromagnetically induced transparency: Optics in coherent media, *Rev. Mod. Phys.* **77**, 633 (2005).
- [17] J. P. Marangos, Electromagnetically induced transparency, *Journal of Modern Optics* **45**, 471 (1998).
- [18] I. Novikova, R. L. Walsworth, and Y. Xiao, Electromagnetically induced transparency-based slow and stored light in warm atoms, *Laser & Photonics Reviews* **6**, 333 (2012).
- [19] A. K. Mohapatra, T. R. Jackson, and C. S. Adams, Coherent optical detection of highly excited rydberg states using electromagnetically induced transparency, *Phys. Rev. Lett.* **98**, 113003 (2007).
- [20] J. D. Pritchard, D. Maxwell, A. Gauguier, K. J. Weatherill, M. P. A. Jones, and C. S. Adams, Cooperative atom-light interaction in a blockaded rydberg ensemble, *Phys. Rev. Lett.* **105**, 193603 (2010).
- [21] D. Petrosyan, J. Otterbach, and M. Fleischhauer, Electromagnetically induced transparency with rydberg atoms, *Phys. Rev. Lett.* **107**, 213601 (2011).
- [22] Comparat, Daniel, Pillet, and Pierre, Dipole blockade in a cold rydberg atomic sample, *Journal of the Optical Society of America B* **27**, A208 (2010).
- [23] A. Browaeys, D. Barredo, and T. Lahaye, Experimental investigations of dipole-dipole interactions between a few rydberg atoms, *Journal of Physics B Atomic Molecular Physics* **49**, 152001 (2016).
- [24] A. Urvoy, F. Ripka, I. Lesanovsky, D. Booth, J. P. Shaffer, T. Pfau, and R. Löw, Strongly correlated growth of rydberg aggregates in a vapor cell, *Phys. Rev. Lett.* **114**, 203002 (2015).
- [25] M. Xiao, Y.-q. Li, S.-z. Jin, and J. Gea-Banacloche, Measurement of dispersive properties of electromagnetically induced transparency in rubidium atoms, *Phys. Rev. Lett.* **74**, 666 (1995).
- [26] I. I. Beterov, I. I. Ryabtsev, D. B. Tretyakov, and V. M. Entin, Quasiclassical calculations of blackbody-radiation-induced depopulation rates and effective lifetimes of rydberg  $ns$ ,  $np$ , and  $nd$  alkali-metal atoms with  $n \leq 80$ , *Phys. Rev. A* **79**, 052504 (2009).
- [27] Q. Zhang, Z. Bai, and G. Huang, Fast-responding property of electromagnetically induced transparency in rydberg atoms, *Phys. Rev. A* **97**, 043821 (2018).
- [28] Y.-W. Guo, S.-L. Xu, J.-R. He, P. Deng, M. R. Belić, and Y. Zhao, Transient optical response of cold rydberg

- atoms with electromagnetically induced transparency, *Phys. Rev. A* **101**, 023806 (2020).
- [29] M. S. Robbins and B. J. Hadwen, The noise performance of electron multiplying charge-coupled devices, *IEEE Transactions on Electron Devices* **50**, 1227 (2003).
- [30] D. Dussault and P. Hoess, Noise performance comparison of ICCD with CCD and EMCCD cameras, in *Infrared Systems and Photoelectronic Technology*, Vol. 5563, edited by C. B. Johnson, E. L. Dereniak, and R. E. Sampson, International Society for Optics and Photonics (SPIE, 2004) pp. 195 – 204.
- [31] D. Petrosyan, M. Höning, and M. Fleischhauer, Spatial correlations of rydberg excitations in optically driven atomic ensembles, *Phys. Rev. A* **87**, 053414 (2013).
- [32] D. Petrosyan, Two-dimensional crystals of rydberg excitations in a resonantly driven lattice gas, *Phys. Rev. A* **88**, 043431 (2013).
- [33] M. Höning, D. Muth, D. Petrosyan, and M. Fleischhauer, Steady-state crystallization of rydberg excitations in an optically driven lattice gas, *Phys. Rev. A* **87**, 023401 (2013).

